Polymer Chemistry

ROYAL SOCIETY OF CHEMISTRY

PAPER

View Article Online
View Journal | View Issue

Check for updates

Cite this: *Polym. Chem.*, 2023, **14**, 4560

# Synthesis and characterization of a ruthenium-containing copolymer for use as a photoredox catalyst†

Steven Huss,[a] Andrew R. Walsh,[b] Anna Griggs,[a] Diego Alejandro Rodriguez-Acevedo,[a] Daniela M. Arias-Rotondo[b] and Elizabeth Elacqua*[a,c]

Received 19th April 2023,
Accepted 1st September 2023

DOI: 10.1039/d3py00428g

rsc.li/polymers

Herein, we report the synthesis and characterization of a PMMA-functionalized copolymer bearing a photoredox-active Ru(II) polypyridyl moiety and pyrene pendant groups. The integration of both the Ru(II) polypyridyl and pyrene pendant groups enabled a photoredox-catalyzed reaction through energy transfer. The effective energy transfer process was evidenced through the polymer's ability to serve as a reductive catalyst toward the formation of carbon–carbon bonds using C–H arylation, wherein product yields ranging from 37–71% were observed. The copolymer design also exhibited solvent-dependent size and catalyst activity, wherein the use of DMSO promoted aggregation of the pyrene groups that led to higher product yield, likely owing to achieving a more confined structure that enables more efficient energy transfer between Ru(II) and pyrene pendant units.

Published on 07 syyskuuta 2023. Downloaded on 6.2.2026 1.24.15.

## Introduction

The success of many photoredox-mediated processes is contingent upon the transfer of electrons from an excited state of a photocatalyst, while the less explored field of energy transfer catalysis revolves around the utilization of photosensitizers that efficiently absorb light and then transfer the energy to other compounds.[1–4] Many metal-based and organic photocatalysts are capable of undergoing energy transfer with suitable molecules to spur reactivity. Moreover, transition metal photocatalysts exhibit a diverse range of photophysical properties and are highly photostable.[5–7] It was recently demonstrated that photoredox through energy transfer occurs in a system comprised of $[Ru(bpy)_3]^{2+}$ (bpy = 2,2′-bipyridine), a highly reducing polycyclic aromatic hydrocarbon (*e.g.*, pyrene or anthracene), and diisopropylethylamine (DIPEA).[8] This proposed system leverages efficient funnelling of the absorbed energy of $[Ru(bpy)_3]^{2+}$ to pyrene (or anthracene) through a triplet energy transfer, likely through a Dexter mechanism,[9] followed by electron transfer between the excited pyrene (or anthracene) and DIPEA. Whereas pyrene and anthracene only absorb in the UV region of the spectrum, using $[Ru(bpy)_3]^{2+}$ allows the reaction to be carried out under milder conditions, because lower-energy light (green or blue) can be used, which is cheaper and safer than UV light, while still accessing the high reductive powers of the polycyclic aromatic hydrocarbons. Several studies have investigated the proposed mechanism, including those led by Ceroni and Balzani, as well as Moore.[10,11] Ceroni and Balzani proposed a sensitized triplet–triplet annihilation upconversion pathway, which was further explored by Wenger using transient absorption and emission spectroscopy methods. Wenger[12] confirmed that the dominant reaction pathway in the sensitization-initiated-ET process is likely to go through a sensitized triplet–triplet annihilation upconversion pathway, consistent with the original postulation by Ceroni and Balzani.

From a sustainability perspective, methods to immobilize precious metal catalysts used in many of these reactions are attractive targets for catalyst design, based on their potential to remove the polymer-based catalyst by simple filtration to isolate and reuse it.[13,14] There are a wide range of commercially available polymer-bound catalysts that can efficiently facilitate a variety of chemical reactions, including palladium-catalyzed cross-coupling reactions,[15,16] Lewis acid-catalyzed reactions,[17,18] amide bond formation,[19,20] and oxidation.[21,22] These catalysts offer a convenient and effective way to perform

[a]*Department of Chemistry, The Pennsylvania State University, University Park, Pennsylvania 16802, USA. E-mail: elizabeth.elacqua@psu.edu*
[b]*Department of Chemistry and Biochemistry, Kalamazoo College, Kalamazoo, Michigan 49006, USA*
[c]*Materials Research Institute, The Pennsylvania State University, University Park, Pennsylvania 16802, USA*

† Electronic supplementary information (ESI) available: Synthetic procedures for monomer and polymer synthesis and characterization. See DOI: https://doi.org/10.1039/d3py00428g


This journal is © The Royal Society of Chemistry 2023

Published on 07 syyskuuta 2023. Downloaded on 6.2.2026 1.24.15.

these reactions in a heterogeneous manner within a laboratory or industrial setting, with the advantage of being able to separate the catalyst easily from the reaction mixture; in some cases, recyclability of the polymer catalyst contributes to a long-term sustainable approach.

Recent avenues toward sustainable polymeric photocatalysis have been demonstrated using both amphiphilic and organic polymer nanoparticles that facilitate photoredox reactions. Specifically, amphiphilic acrylamide-based polymers featuring reductive phenylphenothiazine[23,24] or acridinium[25] pendant units have led to recyclable catalysts. In related studies, oxidative triphenylpyrylium species featured within a poly(methyl methacrylate) (PMMA) backbone have – in concert with polycyclic aromatic hydrocarbon pendant groups – facilitated more efficient single-electron transfer when confined within single-chain polymeric nanoparticles.[26,27] Furthermore, a catalytically-active PMMA was obtained using a self-catalyzed RAFT polymerization of an Eosin Y-based monomer.[28]

## Results and discussion

Motivated both by the photoredox energy transfer system of König[8] and aforementioned homogeneous polymer-based organic photoredox systems, we designed a PMMA backbone with $[Ru(bpy)_3]^{2+}$ and pyrene pendant groups, which serves as a platform for the energy transfer process. Using modified procedures from previous reports, the monomers 1-pyrenemethyl methacrylate[29] and $[Ru(bpy)_2(dmbpy\text{-}MMA)](PF_6)_2$ [30] were synthesized (Fig. 1). A backbone of methyl methacrylate (MMA) was chosen for the photocatalytic polymer due to its solubility in common organic solvents (*e.g.* DCM, MeCN, DMSO, DMF) and its expected similar polymerization kinetics to the 1-pyrenemethyl methacrylate and $[Ru(bpy)_2(dmbpy\text{-}MMA)](PF_6)_2$ comonomers. The ruthenium complex was synthesized and used for the polymerization, rather than in a post-polymerization manner, allowing for controllable incorporation of the photoactive $[Ru(bpy)_2(dmbpy)]^{2+}$ pendant units. The copolymer was prepared through reversible addition–fragmentation chain-transfer (RAFT) polymerization (Fig. 2) using 2,2′-azobis (2-methyl-propionitrile) (AIBN) as an initiator and 4-cyano-4-[(dodecylsulfanylthiocarbonyl)sulfanyl]pentanoic acid as the chain transfer agent. A monomer feed ratio of 10 : 40 : 50 $[Ru(bpy)_2(dmbpy)]^{2+}$ : pyrene : MMA was chosen to achieve a copolymer with a similar Ru(II)/pyrene ratio to that of the energy transfer system of König.[8]

The incorporation of each monomer unit within the resulting copolymer was determined using $^1$H NMR spectroscopy (Fig. S5†), which exhibited broad resonances between 7.0 and 9.0 ppm, assigned to the aromatic protons of the $[Ru(bpy)_2(dmbpy)]^{2+}$ and pyrene pendant groups. The resonance at 8.72 ppm was assigned to six protons from the bipyridine ligands from the $[Ru(bpy)_2(dmbpy)]^{2+}$ group. The broad resonance between 4.8 and 6.0 ppm was assigned to the methylene ($-CH_2-$) protons of both the pyrene and $[Ru(bpy)_2(dmbpy)]^{2+}$ pendant groups. The resonance at 3.54 ppm resulted from the MMA methyl ester. The integration ratios between these three were utilized to estimate the copolymer composition, which revealed the copolymer was comprised of 11.1% $[Ru(bpy)_2(dmbpy)]^{2+}$, 37.5% pyrene, and 51.4% MMA.

The copolymer's poor solubility in several common GPC eluents, such as THF, chloroform, and trichlorobenzene precluded obtaining accurate information on resultant polymer dispersity and molecular weights. Molecular weight was thus characterized using chain-end analysis. To facilitate the analysis, the terminal carboxylic acid was functionalized through esterification with 3-trimethylsilylpropargyl alcohol or pentafluorophenol (see ESI† for further details), which allowed for two different routes to obtain molecular weight. The purified trimethylsilyl propargyl functionalized copolymer exhibited a

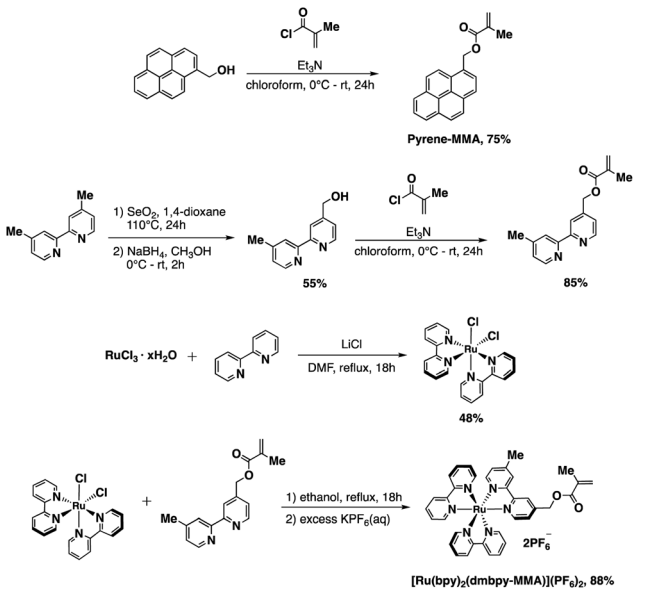


Fig. 1 Synthesis of pyrene methacrylate and ruthenium methacrylate-derivative monomer.

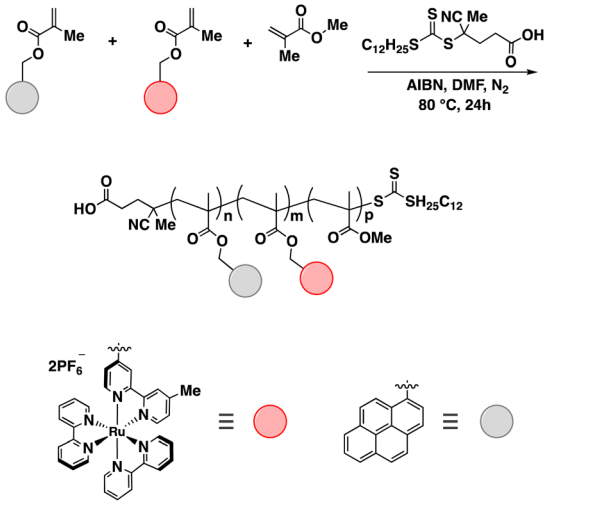


Fig. 2 RAFT polymerization of MMA-based monomers.

Published on 07 syyskuuta 2023. Downloaded on 6.2.2026 1.24.15.

chemical shift at 0.13 ppm resulting from the $-SiMe_3$ group in its $^1$H NMR spectrum; relating this to the integration of other key resonances from the monomeric units (*vide supra*) revealed the copolymer molecular weight to be approximately 29 kDa. The purified pentafluorophenol functionalized copolymer showed three distinct chemical shifts at $\delta = -154.46$, $-160.1$, and $-164.57$ ppm, resulting from the pentafluorobenzene in the $^{19}$F NMR spectrum. Using 1,4-diiodotetrafluorobenzene as an internal standard, we determined the $M_n$ of this copolymer to be approximately 31 kDa. Based on the combined results, the $M_n$ of the copolymer is estimated to be between 29–31 kDa, which is close to the target molecular weight of 30 kDa.

The ruthenium copolymer was characterized using UV-Vis absorption spectroscopy (Fig. S10†). Absorption peaks were observed at wavelengths of 329, 344, and 457 nm, which are similar to those observed in pyrenemethanol (328 and 344 nm)[31] and $[Ru(bpy)_2(dmbpy)](PF_6)_2$ (455 nm).[32] We investigated the photophysical properties of each of the Ru(II) species used in this study, namely, poly[$Ru(bpy)_2(dmbpy)(PF_6)_2$-*co*-pyrene-*co*-MMA], poly[$Ru(bpy)_2(dmbpy)(PF_6)_2$-*co*-MMA], $[Ru(bpy)_2(dmbpy)](PF_6)_2$, and $[Ru(bpy)_2(dmbpy\text{-}MMA)](PF_6)_2$. In addition to the Ru(II) species, we investigated the pyrene species in pyrene, pyrene–MMA, poly[pyrene-*co*-MMA], and poly[$Ru(bpy)_2(dmbpy)(PF_6)_2$-*co*-pyrene-*co*-MMA].

The absorption maxima, molar absorptivity coefficients, singlet energies, and triplet energies were determined for each of the species (Table 1). We observed that the absorption maxima of pyrene in DMSO is very close to that of the pyrene–MMA derivative and its respective polymers; likewise, the singlet energies of pyrene–MMA and its respective polymers are very close in energy to that of small molecule pyrene (~316 kJ mol$^{-1}$ *versus* ~319 kJ mol$^{-1}$). The slight shift in absorbance, and singlet energy, can be explained by the substitution of the weakly sigma donating alkyl group on the pyrene ring system. Nonetheless, the similarity of singlet energies indicates the alkyl group only marginally changes the photophysical properties, and it can be safe to assume that the triplet energy of the pyrene species in pyrene–MMA and on the polymer backbone have a similar triplet energy (or slightly lower) compared to molecular pyrene (~204 kJ mol$^{-1}$ in methylcyclohexane–isopentane 5 : 1 v/v mixture).[54]

We observed that the absorption maxima of the small molecule $[Ru(bpy)_2(dmbpy)](PF_6)_2$ in DMSO is the same as that of $[Ru(bpy)_2(dmbpy\text{-}MMA)](PF_6)_2$ and its respective polymers. Likewise, the singlet and triplet energies are the same between small molecule $[Ru(bpy)_2(dmbpy)](PF_6)_2$ and the $[Ru(bpy)_2(dmbpy\text{-}MMA)](PF_6)_2$-containing polymers. While we were unable to determine the triplet energies of the pyrene species, we observed that the pyrene–MMA and poly[pyrene-*co*-MMA] were able to quench the excited triplet state of Ru(II) in poly[$Ru(bpy)_2(dmbpy)(PF_6)_2$-*co*-MMA] (*vide infra*), suggesting the triplet excited state energy of the pyrene species on the polymer backbone is likely <193 kJ mol$^{-1}$ (Fig. S18†).

The molar absorptivity coefficients of the $[Ru(bpy)_2(dmbpy)](PF_6)_2$ and pyrene species in poly[$Ru(bpy)_2(dmbpy)(PF_6)_2$-*co*-pyrene-*co*-MMA] are lower than that of their monomeric form (~50% less for Ru(II) and ~30% less for pyrene). The molar absorption coefficient decrease for pyrene in monomeric to polymeric form could be evidence of aggregation of pyrene groups as previously observed in literature.[33] This effect is seen to an even greater extent by comparing to the molar absorption coefficient in poly[pyrene-*co*-MMA] in which it decreases to 3390 M$^{-1}$ cm$^{-1}$, likely being from the aggregation of pyrene groups on the polymer backbone.

To ensure that the derivatized Ru(II) and pyrene species on the polymer backbone could be effectively used in the C–H arylation reaction, we performed a Stern–Volmer study with pyrene–MMA (Fig. S18†) to quench the excited triplet state of Ru(II) in poly[$Ru(bpy)_2(dmbpy)(PF_6)_2$-*co*-MMA]. To our delight, the luminescence of $[Ru(bpy)_2(dmbpy)](PF_6)_2$ was effectively quenched by this pyrene species.

We next investigated the photoredox-catalyzed reaction enabled by energy transfer in the C–H arylation of aryl bromides. In a typical experiment, 2 mol% of $[Ru(bpy)_2(dmbpy)](PF_6)_2$ in the Ru-polymer (the weight% of $[Ru(bpy)_2(dmbpy)](PF_6)_2$ in the copolymer was used to determine the amount of Ru-polymer needed; 6.8 mol% pyrene) was dissolved in a suitable solvent ($d_6$-DMSO or MeCN), followed by addition of the aryl bromide, the trapping reagent, and DIPEA. The solution was then sparged with nitrogen for 20 minutes, followed by irradiation with blue light (two Kessil 456 nm LEDs, approximate light-to-vial distance of 6 cm). After 16 hours, 1,3,5-triox-

**Table 1** Photophysical properties of Ru(II) and pyrene species used in this study in DMSO. The molar extinction coefficient given corresponds to the absorption maxima. The singlet energies of the Ru(II) species are estimated from the absorption maxima. The singlet energies of the pyrene species were determined by fitting their fluorescence spectra. The triplet energies of the Ru(II) species were determined by fitting their phosphorescence spectra

| Species | Absorption maxima (nm) | $\varepsilon_{\text{absorption maxima}}$ (M$^{-1}$ cm$^{-1}$) | Singlet energy (kJ mol$^{-1}$, eV) | Triplet energy (kJ mol$^{-1}$, eV) |
|---|---|---|---|---|
| Pyrene | 339 | 46 700 | 319, 3.31 | — |
| Pyrene–MMA | 346 | 35 800 | 316, 3.27 | — |
| $[Ru(bpy)_2(dmbpy)](PF_6)_2$ | 457 | 10 400 | 262, 2.71 | 193, 2.00 |
| $[Ru(bpy)_2(dmbpy\text{-}MMA)](PF_6)_2$ | 457 | 18 400 | 262, 2.71 | 193, 2.00 |
| Poly[$Ru(bpy)_2(dmbpy)(PF_6)_2$-*co*-MMA] | 457 | 12 600 | 262, 2.71 | 193, 2.00 |
| Poly[pyrene-*co*-MMA] | 346 | 3390 | 316, 3.27 | — |
| Poly[$Ru(bpy)_2(dmbpy)(PF_6)_2$-*co*-pyrene-*co*-MMA] | 458 (Ru)<br>344 (Py) | 9350 (Ru)<br>25 200 (Py) | 261, 2.71 (Ru)<br>316, 3.27 (Py) | 193, 2.00 (Ru) |

 This journal is © The Royal Society of Chemistry 2023

Published on 07 syyskuuta 2023. Downloaded on 6.2.2026 1.24.15.

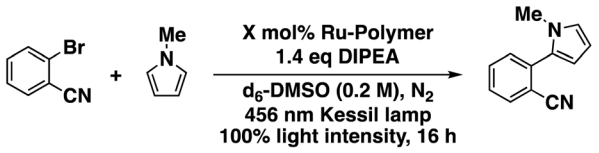


| mol% catalyst | Yield (%) |
|---|---|
| 0.5 | 30 |
| 1 | 46 |
| 2 | 66 |
| 4 | 52 |

**Fig. 3** Yield of 2-(1-methyl-1*H*-pyrrol-2-yl)benzonitrile with varying amounts of $[Ru(dmbpy)(bpy)_2](PF_6)_2$ loadings on polymer backbone.

ane was added to the solution as an internal standard. Product yields were measured through $^1$H NMR spectroscopy. We first screened different catalyst loadings (Fig. 3) using the reaction of 2-bromobenzonitrile and *N*-methylpyrrole as a model system. The highest yield was observed when using a 2 mol% catalyst loading, akin to the findings of König *et al.*, wherein 1 mol% of catalyst was determined to be optimal.

We performed the reaction between 2-bromobenzonitrile and *N*-methylpyrrole screening both MeCN and DMSO as solvents. In the small molecule reaction using 2 mol% $[Ru(bpy)_3](PF_6)_2$ and 5 mol% pyrene, the yields in both acetonitrile and dimethyl sulfoxide are similar after 3 h of stirring in 456 nm LED lights, at 67% and 68%, respectively. In contrast, when the poly[$Ru(bpy)_2(dmbpy)(PF_6)_2$-*co*-pyrene-*co*-MMA] was used as the catalyst, the yields in the two solvent varied significantly, with yields of 54% in acetonitrile and 71% in dimethyl sulfoxide. Since this is only observed when using the copolymer catalyst, it is unlikely to be due to differences in redox potentials of the catalysts between the two solvents as pyrene possesses a first half-wave reduction potential at −2.2 V in MeCN ($E_{1/2}$ (Py/Py$^-$)/V *vs.* SCE)[34a] and at −2.1 V in DMSO ($E_{1/2}$ (Py/Py$^-$)/V *vs.* SCE).[8] Instead, the solvent-dependent yield may be a result of the catalysts being bound to the copolymer backbone. While there should be a difference between the redox potentials between $[Ru(bpy)_3]^{2+}$ and the $[Ru(bpy)_2(dmbpy)]^{2+}$ pendant group, this difference would be relatively small, and its excited-state potential ($E_{1/2}$ Ru(II)*/Ru(III)/V *vs.* SCE = −0.83) would be highly unlikely to reduce ground-state pyrene.[9,34b,35] Thus, the difference in yields may be explained by variations in the proposed energy transfer process between the $[Ru(bpy)_2(dmbpy)]^{2+}$ and pyrene catalysts and/or by differences in the copolymer assembly/aggregation in the two reaction solvents.

To investigate this further, we measured the hydrodynamic radius of the copolymer catalyst in these solvent systems using dynamic light scattering (DLS, Fig. 4). It was found that the copolymer catalyst's hydrodynamic radius is nearly 6 times larger in DMSO than in MeCN. This difference may be caused by some aggregation of the copolymer in DMSO (68 nm *versus* 12 nm). In this scenario, DMSO could act as a poor solvent, promoting strong interactions between individual polymer chains and multiple polymer chains. This could bring the cocatalytic ruthenium complex and pyrene groups closer together, allowing for a more efficient energy transfer process to occur compared to reactions conducted in acetonitrile.[36,37] On the other hand, if acetonitrile acts as a good solvent, the interactions between the polymer and solvent will be stronger than the interactions between the polymer chains, causing the polymer coils to expand and the cocatalytic groups to be farther apart.

We then collected the emission spectra of poly[$Ru(bpy)_2(dmbpy)(PF_6)_2$-*co*-pyrene-*co*-MMA], poly[pyrene-*co*-MMA], and molecular pyrene, using an excitation wavelength of 335 nm, and compared their respective pyrene emissions in the range of 350–650 nm (Fig. 5). Pyrene is a widely recognized fluorophore known for its characteristic excimer emission when pyrene groups come into close proximity or aggregate.[38–41]

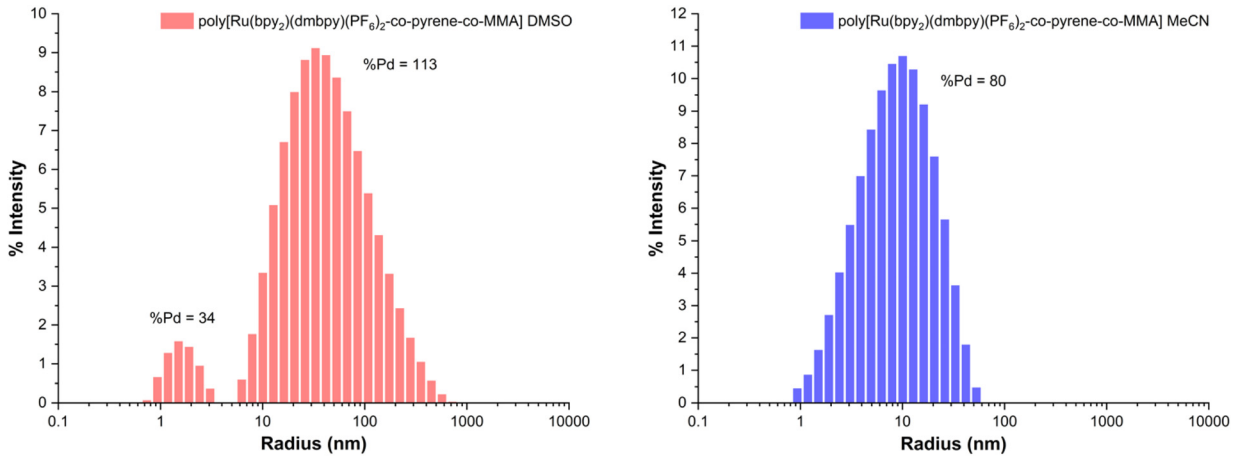


**Fig. 4** Dynamic light scattering (DLS) of poly[$Ru(bpy)_2(dmbpy)(PF_6)_2$-*co*-pyrene-*co*-MMA] in (left) dimethyl sulfoxide (DMSO) and (right) acetonitrile (MeCN).

Published on 07 syyskuuta 2023. Downloaded on 6.2.2026 1.24.15.

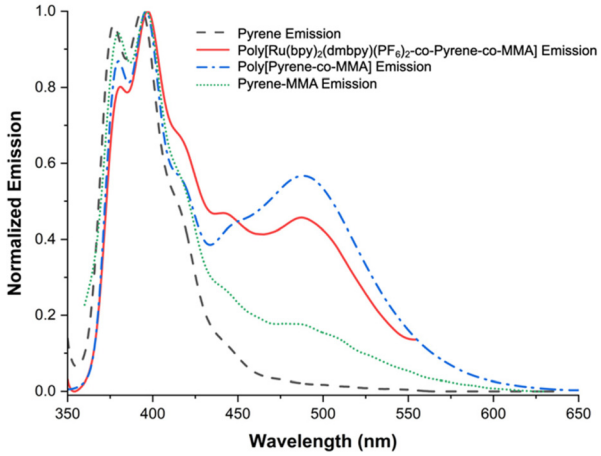


**Fig. 5** Normalized emission spectra of pyrene species used in this study in DMSO; excitation wavelength = 335 nm. The pyrene excimer emission is observed centered at ~488 nm.

The emission spectra of both poly[Ru(bpy)$_2$(dmbpy)(PF$_6$)$_2$-*co*-pyrene-*co*-MMA] and poly[pyrene-*co*-MMA] revealed a significant increase in the intensity of the excimer emission band at ~488 nm when excited at 335 nm in DMSO; this observation indicates the formation of pyrene excimers in both copolymers. In conjunction with DLS data, this provides additional evidence that the pyrene groups are in close proximity and/or aggregating in the DMSO solution. The higher relative intensity of the excimer emission, compared to that of the pyrene emission centered at ~385 nm, in the spectrum of poly [pyrene-*co*-MMA] suggests a greater aggregation of the pyrene groups. This can be attributed to the hydrophobic nature of the copolymer, which facilitates stronger aggregation in the polar DMSO solution. Additionally, when dissolved in acetonitrile, the pyrene excimer emission is both less intense and less distinct, suggesting reduced aggregation or increased spatial separation of the pyrene groups (Fig. S19†). Furthermore, the absence of the excimer emission in molecular pyrene (in DMSO) supports the notion that its formation relies heavily on the diffusion and local concentration of pyrene molecules. Pyrene molecules can freely diffuse in the DMSO solution, lessening their local concentration.

The presence of pyrene aggregation has been qualitatively estimated before by measuring the peak-to-valley ratio taken as the ratio of the absorbance at the ~344 nm maximum over that of the ~334 nm valley.[42,43] This has been characterized before from the knowledge that a peak-to-valley value larger than 3 is indicative of the absence of pyrene aggregates in solution, and *vice versa*. This analysis using the UV-Vis spectra of poly[Ru(bpy)$_2$(dmbpy)(PF$_6$)$_2$-*co*-pyrene-*co*-MMA] in both MeCN and DMSO (Fig. S10†) gave peak-to-valley ratios of 1.93 in acetonitrile and 1.49 in DMSO. In the monomeric form, pyrene–MMA has a peak-to-valley ratio of 3.15. These values, being less than 3.15, indicate that the pyrene groups in both solvents do in fact aggregate but to a lesser extent in MeCN.

We sought to assess the effectiveness of the copolymer catalyst for the C–H arylation of a range of aryl bromides and radical traps, with yields generally ranging between 37–71% (Fig. 6), with most reaction yields plateauing around 16 hours. The longer reaction times compared to the small molecule catalyst counterparts (16 hours *versus* 3 hours) may be due, in part, to the fact that the ruthenium complex used in the copolymer is a [Ru(bpy)$_2$(dmbpy)]$^{2+}$ derivative which may affect the yield. In the [4 + 2] cycloaddition between *trans*-anethole and isoprene, for instance, it was shown that the dimethylbipyridine-based complex achieved lessened yields compared to [Ru(bpy)$_3$](PF$_6$)$_2$ in the same reaction time.[32] In addition to this, the polymer aggregation may also limit access of the substrates to the catalytic groups. In general, aryl bromides with electron withdrawing substituents worked well with the poly[Ru(bpy)$_2$(dmbpy)(PF$_6$)$_2$-*co*-pyrene-*co*-MMA] catalyst in the arylation reactions. As a control, 4-bromoanisole and *N*-methylpyrrole were subjected to the same reaction conditions, where no product was observed. The electron-donating methoxy group on 4-bromoanisole lowers its reduction potential to −2.6 V,[44] which is too low for the pyrene radical anion (reductive potential of −2.1 V)[8] to reduce it.

In addition, we used combinations of 2 mol% Ru(II) and 4 mol% pyrene species as controls between the reaction of 2-bromobenzonitrile and *N*-methylpyrrole. We found that using poly[Ru(bpy)$_2$(dmbpy)(PF$_6$)$_2$-*co*-MMA] and poly[pyrene-*co*-MMA] gave a product yield of 42%; this likely indicates that the excited Ru(II) species have hindered access to the pyrene groups due to polymer aggregation observed within the poly [pyrene-*co*-MMA] copolymer. Use of [Ru(bpy)$_2$(dmbpy-MMA)] (PF$_6$)$_2$ and pyrene–MMA monomers in the reaction gave a lowered yield of 27%, which is likely in part due to the competing polymerization of the monomer groups during the reaction. The combination of these results support the notion that having both the Ru(II) and pyrene species on the same polymer backbone is a crucial factor for achieving high reaction yields.

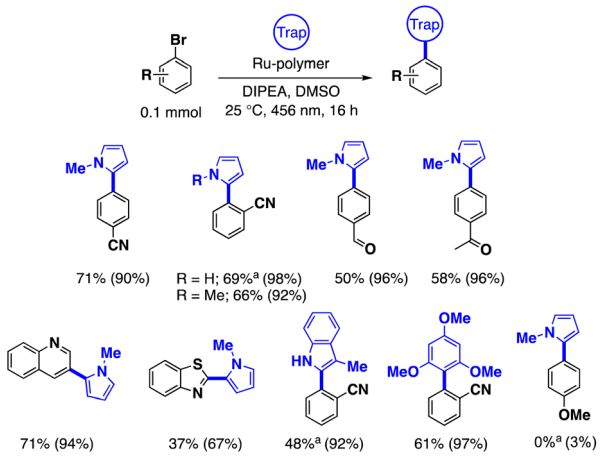


**Fig. 6** The C–H arylation products obtained from (hetero)aryl bromides and heterocycles. Yields are determined by $^1$H NMR spectroscopy using 1,3,5-trioxane as an internal standard. Parentheses indicate the percent conversion of the aryl bromide. [a] Reaction time was 32 hours.

 This journal is © The Royal Society of Chemistry 2023

Published on 07 syyskuuta 2023. Downloaded on 6.2.2026 1.24.15.

An on/off light experiment (Fig. 7) during the reaction between 4-bromobenzonitrile and *N*-methylpyrrole shows that light is necessary for the reaction to proceed, as product yield does not increase when the LED lights are off. This is in good agreement with a control reaction in which no product formation was observed when the reaction was performed in the dark. It also shows that the yield of the reaction between 2-bromobenzonitrile and *N*-methylpyrrole begins to plateau at around 16 hours of total light exposure time. As the reaction proceeds, we observe a gradual decrease in its rate, noticeable from the decreased slope of the reaction yield between 4–6 hours. Given this trend, we sought to investigate the catalyst fidelity over the course of the reaction to determine if this is evidence of catalyst degradation.

Throughout the reaction between 4-bromobenzonitrile and *N*-methylpyrrole, aliquots were taken, and their UV-Vis spectra were collected (Fig. 8 and S24†). As the reaction progressed, we observed a marked increase in intensity within the 300–375 nm range, which corresponds to the anticipated formation of the 4-(1-methyl-1*H*-pyrrol-2-yl)benzonitrile product.[45] Additionally, we noted a decrease in the absorption at 454 nm, which corresponds to the $[Ru(bpy)_2(dmbpy)]^{2+}$ complex present in the copolymer, providing evidence of the complex degrading during the course of the reaction.

Following the reaction, the copolymers were reprecipitated in both benzene and hexanes. Upon analysis of the resulting copolymers using UV-Vis spectroscopy (Fig. 9 and S24†), we observed a significant reduction in the main absorption peak of the $[Ru(bpy)_2(dmbpy)]^{2+}$ complex at 454 nm and the emergence of a new absorption peak centered at 429 nm. This suggests that a portion of the $[Ru(bpy)_2(dmbpy)]^{2+}$ complexes had dissociated under blue light irradiation. Prior reports demonstrate that $[Ru(bpy)_3]^{2+}$ complexes can undergo photochemical decomposition upon light irradiation, which can be a major obstacle in photocatalysis.[46–51] In the region of 275–375 nm, there is evidence for the preservation of a portion of the pyrene groups at 329 and 344 nm; however, broad absorbances observed in this region give further indication of the polymer degradation. One such possibility could be from the radical coupling of the pyrene groups to form a 1,1′-bipyrene species which also exhibits absorbances in this region.[52] Furthermore, we note that photodegradation of the $[Ru(bpy)_2(dmbpy)]^{2+}$ complex within poly[$Ru(bpy)_2(dmbpy)(PF_6)_2$-*co*-pyrene-*co*-MMA] copolymer is observed using UV-Vis spectroscopy when it is exposed to 456 nm lights under reaction conditions, but in the absence of substrates or reagents, over 16 hours (Fig. S21†). There is notable decrease in the MLCT absorbance with longer exposure times. A similar trend is also

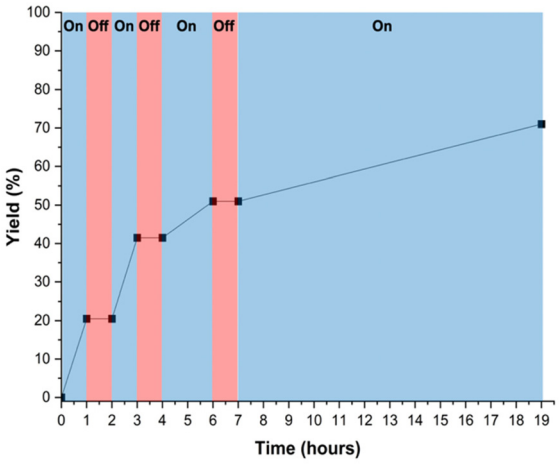


Fig. 7 On/off light study during conversion of 4-bromobenzontirile and *N*-methylpyrrole to 4-(1-methyl-1*H*-pyrrol-2-yl)benzonitrile catalyzed by poly[$Ru(bpy)_2(dmbpy)(PF_6)_2$-*co*-pyrene-*co*-MMA], demonstrating that during the periods of time where the lights are off, the reaction pauses and the reaction continues with the lights on.

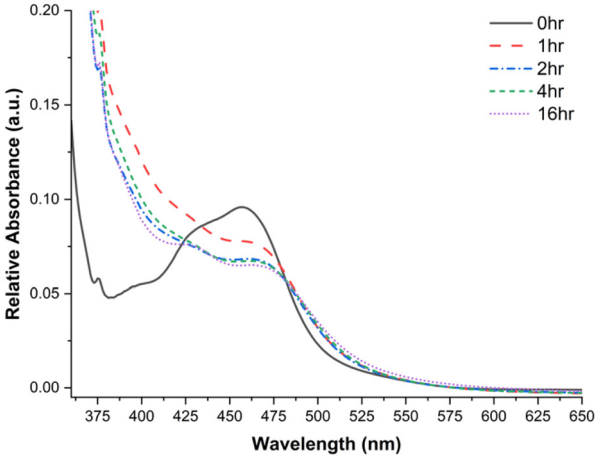


Fig. 8 UV-Vis spectra in DMSO obtained during the reaction of 4-bromobenzontirile and *N*-methylpyrrole demonstrating progressive decrease in the fidelity of the Ru(II) complex. The spectra were collected at identical concentrations.

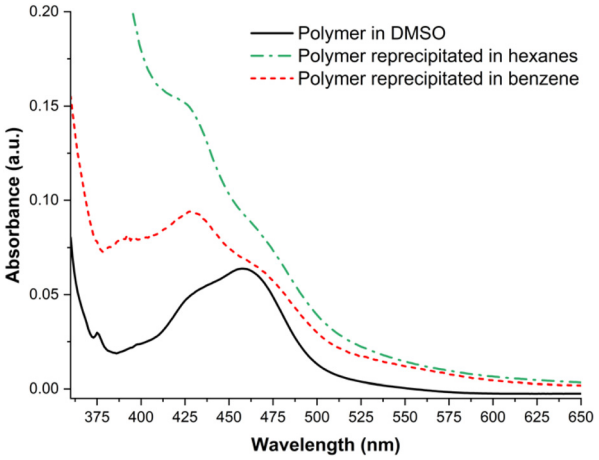


Fig. 9 UV-Vis spectra of poly[$Ru(bpy)_2(dmbpy)(PF_6)_2$-*co*-pyrene-*co*-MMA] in DMSO reprecipitated in hexanes and benzene after reaction between 4-bromobenzontirile and *N*-methylpyrrole. The spectra were collected at variable concentrations of copolymer.

Published on 07 syyskuuta 2023. Downloaded on 6.2.2026 1.24.15.

observed when a mixture of $[Ru(bpy)_2(dmbpy)](PF_6)_2$ and pyrene is dissolved under reaction conditions and exposed to 456 nm light over 16 hours (Fig. S20†). The combination of these results show that the polymer (and small molecule catalyst) can degrade under 456 nm light even in the absence of reagents and that the photodegradation of the $[Ru(bpy)_2(dmbpy)]^{2+}$ complex is not a result of it being a part of the copolymer system.

A separate reaction between 2-bromobenzonitrile and the trapping agent 1,3,5-trimethoxybenzene was performed at a larger scale, wherein a yield of 57% was obtained. After removing the solvent, reprecipitating the polymer in diethyl ether, and drying the polymer under reduced pressure, a $^1$H NMR spectrum was obtained of the recovered polymer (Fig. S23†). It was observed that methylene ($-CH_2-$) proton peaks (5–6 ppm) were not present in the spectrum. This likely indicates that the pyrene and possibly the ruthenium complex degrade during the reaction.[47–50] Specifically, the bpy ligand can dissociate from the complex, and potentially form a $[Ru(bpy)(dmbpy)(X)]^{2+}$ pendant group. The presence of the peak with a chemical shift at ~10.1 ppm in the $^1$H NMR spectrum (Fig. S23†) further suggests the ruthenium complex is likely photodissociating through loss of one bipyridine ligand, possibly forming a $[Ru(bpy)(dmbpy)(DMSO)_2]^{2+}$ pendant group.[53] In turn, this could also suggest that the dmbpy group may photodissociate as well, and the ruthenium metal may leach off the polymer backbone. When this polymer was used in a second cycle of the reaction, only trace amounts of the product were obtained, suggesting degradation of the Ru-polymer during the reaction. The different rates of product formation observed in the on/off studies and the general plateauing of product formation, thus, are likely explained by the photo-induced decomposition of the polymer during the reaction.

## Conclusions

We synthesized a poly(methyl methacrylate) copolymer bearing $[Ru(bpy)_2(dmbpy)]^{2+}$ groups through RAFT polymerization. These results demonstrate that a poly[$Ru(bpy)_2(dmbpy)(PF_6)_2$-*co*-pyrene-*co*-MMA] copolymer can effectively catalyze the activation of (hetero)aryl halides toward the formation of carbon–carbon bonds through C–H arylation, yielding good results for electron-deficient substrates.

The copolymer also exhibited a solvent-dependent size in acetonitrile and dimethyl sulfoxide, as well as solvent-dependent catalytic activity. This is likely owing to the presence of stronger polymer–polymer interactions in DMSO compared to stronger polymer–solvent interactions being dominant in MeCN. The former interactions likely lead to a more confined structure being promoted through aggregation of the copolymer in DMSO. Aggregation of the pyrene groups was confirmed through observing the excimer within the copolymer's emission spectra, in addition to a significantly decreased peak-to-valley ratio of the pyrene absorbance in the copolymer's UV-Vis spectrum. This observed aggregation is thought to bring the cocatalytic groups closer together and allow for a more efficient energy transfer process to occur.

Efforts to comprehend the plateauing catalyst activity/reactivity led to observations that the fidelity of the copolymer catalyst was compromised during the reaction, likely owing to photodissociation. While the mechanism of the photodissociation is unknown, it could potentially be from either the reduction of the ester group, subsequent cleavage of the pyrene unit, or through deprotonation of the slightly more acidic methylene group. To address the overall photostability issue, further photocatalytic copolymer designs comprising ruthenium-based complexes will feature less labile ligands. This will not only prevent photodissociation, but allow for a potential recyclable, photoredox-active metal complex-containing copolymer to be achieved.

## Conflicts of interest

There are no conflicts to declare.

## Acknowledgements

This work was supported by the National Science Foundation Early CAREER program (CHE-2046470) and Research Experience for Undergraduates Program (CHE-2050927). The authors also acknowledge support from the Alfred P. Sloan Foundation (FG-2021-15490) and start-up funds generously provided by Kalamazoo College and the Pennsylvania State University.

## References

1 F. Strieth-Kalthoff and F. Glorius, Triplet Energy Transfer Photocatalysis: Unlocking the Next Level, *Chem*, 2020, **6**(8), 1888–1903.
2 F. Strieth-Kalthoff, M. J. James, M. Teders, L. Pitzer and F. Glorius, Energy Transfer Catalysis Mediated by Visible Light: Principles, Applications, Directions, *Chem. Soc. Rev.*, 2018, **47**(19), 7190–7202.
3 N. A. Till, L. Tian, Z. Dong, G. D. Scholes and D. W. C. MacMillan, Mechanistic Analysis of Metallaphotoredox C–N Coupling: Photocatalysis Initiates and Perpetuates Ni(I)/Ni(III) Coupling Activity, *J. Am. Chem. Soc.*, 2020, **142**(37), 15830–15841.
4 E. R. Welin, C. Le, D. M. Arias-Rotondo, J. K. McCusker and D. W. C. MacMillan, Photosensitized, Energy Transfer-Mediated Organometallic Catalysis through Electronically Excited Nickel(II), *Science*, 2017, **355**(6323), 380–385.
5 R. Bevernaegie, S. A. M. Wehlin, E. J. Piechota, M. Abraham, C. Philouze, G. J. Meyer, B. Elias and L. Troian-Gautier, Improved Visible Light Absorption of Potent Iridium(III) Photo-Oxidants for Excited-State Electron Transfer Chemistry, *J. Am. Chem. Soc.*, 2020, **142**(6), 2732–2737.

 This journal is © The Royal Society of Chemistry 2023

Published on 07 syyskuuta 2023. Downloaded on 6.2.2026 1.24.15.

6 I. N. Mills, J. A. Porras and S. Bernhard, Judicious Design of Cationic, Cyclometalated Ir(III) Complexes for Photochemical Energy Conversion and Optoelectronics, *Acc. Chem. Res.*, 2018, **51**(2), 352–364.
7 K. Teegardin, J. I. Day, J. Chan and J. Weaver, Advances in Photocatalysis: A Microreview of Visible Light Mediated Ruthenium and Iridium Catalyzed Organic Transformations, *Org. Process Res. Dev.*, 2016, **20**(7), 1156–1163.
8 I. Ghosh, R. S. Shaikh and B. König, Sensitization-Initiated Electron Transfer for Photoredox Catalysis, *Angew. Chem., Int. Ed.*, 2017, **56**(29), 8544–8549.
9 D. M. Arias-Rotondo and J. K. McCusker, The Photophysics of Photoredox Catalysis: A Roadmap for Catalyst Design, *Chem. Soc. Rev.*, 2016, **45**(21), 5803–5820.
10 M. Marchini, G. Bergamini, P. G. Cozzi, P. Ceroni and V. Balzani, Photoredox Catalysis: The Need to Elucidate the Photochemical Mechanism, *Angew. Chem., Int. Ed.*, 2017, **56**(42), 12820–12821.
11 M. S. Coles, G. Quach, J. E. Beves and E. G. Moore, A Photophysical Study of Sensitization–Initiated Electron Transfer: Insights into the Mechanism of Photoredox Activity, *Angew. Chem., Int. Ed.*, 2020, **59**(24), 9522–9526.
12 F. Glaser, C. Kerzig and O. S. Wenger, Sensitization-Initiated Electron Transfer via Upconversion: Mechanism and Photocatalytic Applications, *Chem. Sci.*, 2021, **12**(29), 9922–9933.
13 J. Ma, F. Strieth-Kalthoff, T. Dalton, M. Freitag, J. L. Schwarz, K. Bergander, C. Daniliuc and F. Glorius, Direct Dearomatization of Pyridines via an Energy-Transfer-Catalyzed Intramolecular [4 + 2] Cycloaddition, *Chem*, 2019, **5**(11), 2854–2864.
14 D. Friedmann, A. Hakki, H. Kim, W. Choi and D. Bahnemann, Heterogeneous Photocatalytic Organic Synthesis: State-of-the-Art and Future Perspectives, *Green Chem.*, 2016, **18**(20), 5391–5411.
15 S.-B. Jang, Polymer-Bound Palladium-Catalyzed Cross-Coupling of Organoboron Compounds with Organic Halides and Organic Triflates, *Tetrahedron Lett.*, 1997, **38**(10), 1793–1796.
16 Y. Uozumi, H. Danjo and T. Hayashi, Cross-Coupling of Aryl Halides and Allyl Acetates with Arylboron Reagents in Water Using an Amphiphilic Resin-Supported Palladium Catalyst, *J. Org. Chem.*, 1999, **64**(9), 3384–3388.
17 L. Yu, D. Chen, J. Li and P. G. Wang, Preparation, Characterization, and Synthetic Uses of Lanthanide(III) Catalysts Supported on Ion Exchange Resins, *J. Org. Chem.*, 1997, **62**(11), 3575–3581.
18 T. Masquelin, H. Bui, B. Brickley, G. Stephenson, J. Schwerkoske and C. Hulme, Sequential Ugi/Strecker Reactions via Microwave Assisted Organic Synthesis: Novel 3-Center-4-Component and 3-Center-5-Component Multi-Component Reactions, *Tetrahedron Lett.*, 2006, **47**(17), 2989–2991.
19 R. J. Booth and J. C. Hodges, Polymer-Supported Quenching Reagents for Parallel Purification, *J. Am. Chem. Soc.*, 1997, **119**(21), 4882–4886.
20 C. Blackburn, B. Guan, P. Fleming, K. Shiosaki and S. Tsai, Parallel Synthesis of 3-Aminoimidazo[1,2-a]Pyridines and Pyrazines by a New Three-Component Condensation, *Tetrahedron Lett.*, 1998, **39**(22), 3635–3638.
21 G. Cardillo, M. Orena and S. Sandri, Polymer Supported Reagents. Chromic Acid on Anion Exchange Resin Synthesis of Aldehydes and Ketones from Allylic and Benzylic Halides, *Tetrahedron Lett.*, 1976, **17**(44), 3985–3986.
22 G. Cainelli, G. Cardillo, M. Orena and S. Sandri, Polymer Supported Reagents. Chromic Acid on Anion Exchange Resins. A Simple and Practical Oxidation of Alcohols to Aldehydes and Ketones, *J. Am. Chem. Soc.*, 1976, **98**(21), 6737–6738.
23 F. Eisenreich and A. R. A. Palmans, Direct C–H Trifluoromethylation of (Hetero)Arenes in Water Enabled by Organic Photoredox–Active Amphiphilic Nanoparticles, *Chem. – Eur. J.*, 2022, **28**, e202201322.
24 F. Eisenreich, E. W. Meijer and A. R. A. Palmans, Amphiphilic Polymeric Nanoparticles for Photoredox Catalysis in Water, *Chem. – Eur. J.*, 2020, **26**(45), 10355–10361.
25 F. Eisenreich, T. H. R. Kuster, D. van Krimpen and A. R. A. Palmans, Photoredox-Catalyzed Reduction of Halogenated Arenes in Water by Amphiphilic Polymeric Nanoparticles, *Molecules*, 2021, **26**(19), 5882.
26 J. J. Piane, L. E. Chamberlain, S. Huss, L. T. Alameda, A. C. Hoover and E. Elacqua, Organic Photoredox-Catalyzed Cycloadditions Under Single-Chain Polymer Confinement, *ACS Catal.*, 2020, **10**(22), 13251–13256.
27 J. J. Piane, S. Huss, L. T. Alameda, S. J. Koehler, L. E. Chamberlain, M. J. Schubach, A. C. Hoover and E. Elacqua, Single–chain Polymers as Homogeneous Oxidative Photoredox Catalysts, *J. Polym. Sci.*, 2021, **59**(22), 2867–2877.
28 J. J. Lessard, G. M. Scheutz, A. B. Korpusik, R. A. Olson, C. A. Figg and B. S. Sumerlin, Self-Catalyzing Photoredox Polymerization for Recyclable Polymer Catalysts, *Polym. Chem.*, 2021, **12**(15), 2205–2209.
29 A. H. Lebovitz, K. Khait and J. M. Torkelson, In Situ Block Copolymer Formation during Solid-State Shear Pulverization: An Explanation for Blend Compatibilization via Interpolymer Radical Reactions, *Macromolecules*, 2002, **35**(26), 9716–9722.
30 P. Yuan, O. Kuksenok, D. E. Gross, A. C. Balazs, J. S. Moore and R. G. Nuzzo, UV Patternable Thin Film Chemistry for Shape and Functionally Versatile Self-Oscillating Gels, *Soft Matter*, 2013, **9**(4), 1231–1243.
31 J. G. Domínguez Chávez, S. H. Ortega and M. Martinez-Garcia, Synthesis of Pyrene-Anthracene Conjugated Molecular Rods, *Open Org. Chem. J.*, 2009, **3**(1), 11–21.
32 S. S. Rozenel, C. R. Azpilcueta, M. M. Flores-Leonar, J. P. F. Rebolledo-Chávez, L. Ortiz-Frade, C. Amador-Bedolla and E. Martin, Ruthenium Tris Bipyridine Derivatives and Their Photocatalytic Activity in [4 + 2]

Published on 07 syyskuuta 2023. Downloaded on 6.2.2026 1.24.15.

Cycloadditions. An Experimental and DFT Study, *Catal. Today*, 2018, **310**, 2–10.

33 H. Siu and J. Duhamel, Molar Absorption Coefficient of Pyrene Aggregates in Water, *J. Phys. Chem. B*, 2008, **112**, 15301–15312.

34 (*a*) C. Koper, M. Sarobe and L. W. Jenneskens, Redox Properties of Non-Alternant Cyclopenta-Fused Polycyclic Aromatic Hydrocarbons: The Effect of Peripheral Pentagon Annelation, *Phys. Chem. Chem. Phys.*, 2004, **6**(2), 319–327; (*b*) P. A. Mabrouk and M. S. Wrighton, Resonance Raman Spectroscopy of the Lowest Excited State of Derivatives of Tris(2,2′-Bipyridine)Ruthenium(II): Substituent Effects on Electron Localization in Mixed-Ligand Complexes, *Inorg. Chem.*, 1986, **25**(4), 526–531.

35 L. Geren, B. Durham and F. Millett, Use of Ruthenium Photoreduction Techniques to Study Electron Transfer in Cytochrome Oxidase, in *Methods in Enzymology*, Academic Press, 2009, pp. 507–520.

36 S. Speiser, Photophysics and Mechanisms of Intramolecular Electronic Energy Transfer in Bichromophoric Molecular Systems: Solution and Supersonic Jet Studies, *Chem. Rev.*, 1996, **96**(6), 1953–1976.

37 S. S. Skourtis, C. Liu, P. Antoniou, A. M. Virshup and D. N. Beratan, Dexter Energy Transfer Pathways, *Proc. Natl. Acad. Sci. U. S. A.*, 2016, **113**(29), 8115–8120.

38 S. S. Lehrer, Intramolecular Pyrene Excimer Fluorescence: A Probe of Proximity and Protein Conformational Change, in *Methods in Enzymology*, Academic Press, 1997, pp. 286–295.

39 J. Duhamel, 7 - Pyrene Fluorescence to Study Polymeric Systems, in *Molecular Interfacial Phenomena of Polymers and Biopolymers*, ed. P. Chen, Woodhead Publishing, 2005, pp. 214–248.

40 G. K. Bains, S. H. Kim, E. J. Sorin and V. Narayanaswami, The Extent of Pyrene Excimer Fluorescence Emission Is a Reflector of Distance and Flexibility: Analysis of the Segment Linking the LDL Receptor-Binding and Tetramerization Domains of Apolipoprotein E3, *Biochemistry*, 2012, **51**(31), 6207–6219.

41 R. Casier and J. Duhamel, Pyrene Excimer Fluorescence as a Direct and Easy Experimental Means to Characterize the Length Scale and Internal Dynamics of Polypeptide Foldons, *Macromolecules*, 2018, **51**(9), 3450–3457.

42 F. M. Winnik, Photophysics of Preassociated Pyrenes in Aqueous Polymer Solutions and in Other Organized Media, *Chem. Rev.*, 1993, **93**(2), 587–614.

43 S. Pirouz and J. Duhamel, New Approaches to Characterize Polymeric Oil Additives in Solution Based on Pyrene Excimer Fluorescence, *J. Polym. Sci., Part B: Polym. Phys.*, 2017, **55**(1), 7–18.

44 A. A. Isse, P. R. Mussini and A. Gennaro, New Insights into Electrocatalysis and Dissociative Electron Transfer Mechanisms: The Case of Aromatic Bromides, *J. Phys. Chem. C*, 2009, **113**(33), 14983–14992.

45 S. Murali, P. Changenet-Barret, C. Ley, P. Plaza, W. Rettig, M. M. Martin and R. Lapouyade, Photophysical Properties of Pyrrolobenzenes with Different Linking and Substitution Pattern: The Transition between Charge Transfer States with Large (MICT) and Small (TICT) Resonance Interaction, *Chem. Phys. Lett.*, 2005, **411**(1–3), 192–197.

46 D. W. Thompson, A. Ito and T. J. Meyer, $[Ru(Bpy)_3]^{2+*}$ and Other Remarkable Metal-to-Ligand Charge Transfer (MLCT) Excited States, *Pure Appl. Chem.*, 2013, **85**(7), 1257–1305.

47 J. K. White, R. H. Schmehl and C. Turro, An Overview of Photosubstitution Reactions of Ru(II) Imine Complexes and Their Application in Photobiology and Photodynamic Therapy, *Inorg. Chim. Acta*, 2017, **454**, 7–20.

48 E. T. Luis, H. Iranmanesh and J. E. Beves, Photosubstitution Reactions in Ruthenium(II) Trisdiimine Complexes: Implications for Photoredox Catalysis, *Polyhedron*, 2019, **160**, 1–9.

49 J. Wang, S. Zhou, B. Li, X. Liu, H. Chen and H. Wang, Improving the Photostability of $[Ru(Bpy)_3]^{2+}$ by Embedment in Silica, *ChemPhotoChem*, 2022, **6**(10), e202200124.

50 J.-M. Lehn and R. Ziessel, Photochemical Reduction of Carbon Dioxide to Formate Catalyzed by 2,2′-Bipyridine- or 1,10-Phenanthroline-Ruthenium(II) Complexes, *J. Organomet. Chem.*, 1990, **382**(1–2), 157–173.

51 S. Jiang, J. Liu, K. Zhao, D. Cui, P. Liu, H. Yin, M. Al-Mamun, S. E. Lowe, W. Zhang, Y. L. Zhong, J. Chen, Y. Wang, D. Wang and H. Zhao, $Ru(Bpy)_3{}^{2+}$-Sensitized {001} Facets $LiCoO_2$ Nanosheets Catalyzed $CO_2$ Reduction Reaction with 100% Carbonaceous Products, *Nano Res.*, 2022, **15**(2), 1061–1068.

52 V. A. Nefedov, Pyrene Dimerization into 1,1′-Dipyrenyl, *Russ. J. Org. Chem.*, 2007, **43**(8), 1163–1166.

53 J. J. Rack and N. V. Mockus, Room-Temperature Photochromism in Cis - and Trans -$[Ru(Bpy)_2(DMSO)_2]^{2+}$, *Inorg. Chem.*, 2003, **42**(19), 5792–5794.

54 W. G. Herkstroeter, A. A. Lamola and G. S. Hammond, Mechaisms of Photochemical Reactions in Solution. XXVIII.[1] Values of Triplet Excitation energies of Selected Sensitizers, *J. Am. Chem. Soc.*, 1964, **86**(21), 4537–4540.

 This journal is © The Royal Society of Chemistry 2023